SMAR 2019 – Fifth Conference on Smart Monitoring,
Assessment and Rehabilitation of Civil Structures

SMAR 2019

Behavior of iron-based shape memory alloys under cyclic loading histories

Diego Isidoro HEREDIA ROSA[1], Alexander HARTLOPER[1], Albano SOUSA [1],
Dimitrios LIGNOS[1], Masoud MOTAVALLI[2], Elyas GHAFOORI[2]
[1] Ecole Polytechnique Fédérale de Lausanne (EPFL), Lausanne, Switzerland
[2] Swiss Federal Laboratories for Material Science and Technology
(Empa), Dübendorf, Switzerland

Contact e-mail: diego.herediarosa@epfl.ch

ABSTRACT: Shape memory alloys (SMAs) have gained considerable attention in a broad range of engineering applications. In particular, iron-based SMAs (Fe-SMAs) have been recently developed and used as a cost-effect method for prestressed-strengthening of civil structures. Previous studies have shown that Fe-SMA offers a strong shape memory effect (SME), however, a negligible superelastic behavior. The potential use of Fe-SMAs in seismic design and retrofit applications including supplemental damping is not yet clear and requires the further understanding of the material behavior under large amplitude cyclic inelastic straining. This study discusses key findings from a material-level experimental program that involved Fe-SMA round coupons subjected to a broad range of uniaxial cyclic strain histories representative of earthquake loading. The Fe-SMA material properties associated with its nonlinear behavior, including cyclic hardening are discussed.

1 INTRODUCTION

Shape memory alloys (SMAs) are materials that after achieving large deformations can return to a predefined shape after unloading or upon heating. The principal mechanism involved in this phenomenon is a reversible phase transformation that SMAs undergo. The phase transformation consists in the change of the crystal structure of a material. It is caused either by a change in temperature or by imposing a stress field. The transformation can manifest in two types of responses: (1) superelasticity, as observed by a flag-shaped hysteresis, and (2) shape memory effect, in which the material is able to return to its original configuration after activation (*e.g.* with temperature). Applications of these materials are widespread. Examples in civil engineering can be found in the use of shape memory effects for prestressing concrete (Czaderski et al. 2015), and super-elasticity for energy dissipation in seismic applications (Miller et al. 2012, Speicher, et al. 2011 and McCormick et al. 2007). Iron-based (Fe-)SMAs are used for their lower cost compared to other SMAs, while still retaining shape memory effect properties.

With respect to the use of SMAs for seismic applications, it is essential to understand the material's behavior under uniaxial cyclic tension/compression loading. Earthquake loading is naturally erratic and, consequently, characterizing material response under a rich set of imposed strain demands is a necessity. While Ni-Ti SMAs have been extensively studied under uniaxial cyclic straining, this is not the case for Fe-SMAs, even though some applications have been reported for seismic purposes (Sawaguchi et al., 2016) . Other aspects, such as the fatigue behavior of Fe-SMAs, have been studied more thoroughly (Sawaguchi et al. 2015; Nikulin et al.

2013; Nikulin et al. 2016; Nikulin et al. 2014). However, the composition of the Fe-SMA used in the above studies is not the same as the one described in this paper. Moreover, the employed loading histories in the aforementioned studies were not representative of earthquake events. Pertinent studies on an Fe-SMA with nominally identical composition can be found in Ghafoori et al. (2017) and Lee et al. (2013), including relevant work by some of the authors under cyclic loading in Hosseini et al. (2018).

This paper presents current progress in a series of tests conducted in EPFL's Structures Laboratory (GIS) facilities to characterize the behavior of Fe-SMAs under uniaxial inelastic cyclic straining. The Fe-SMA studied in this paper is the same as in Lee et al. (2013), that is the Fe-17Mn-5Si-10Cr-4Ni-1(V,C) (ma,-%), which will be hereafter referred to as Fe-SMA. The load protocols and the strain ranges focus on the specificities related to seismic loading, with high compressive strains and strain rates consistent with those observed in full-scale component tests under cyclic loading (e.g., Elkady & Lignos, 2018).

2 METHODOLOGY

2.1 Experimental setup

This section discusses the experimental setup used to conduct the uniaxial cyclic tension/compression tests to characterize the material behavior of the Fe-SMA. Figures 1(a) and 1(b) show the test apparatus and a detailed view of the specimen inside the testing machine, respectively, including the different measurement devices.

The testing machine shown in Figure 1(a) is a Schenk self-reacting frame with the cross-beam controlled by an electric actuator. Two cameras are used to record multiple steps of each loading excursion, should buckling of the specimen occur. Figure 1(b) illustrates the inner part of the setup which consists of an MTS extensometer with a gauge length, L_0 = 8 mm and a PT100 sensor used to measure the surface temperature of the specimen. The specimens used are smooth round bar coupons designed to delay buckling of the specimen to large compressive strains. The unreduced diameter is 12 mm (with M12 threading). The diameter of the reduced section is 8 mm. More details on the setup within the test rig can be found in De Castro e Sousa & Lignos (2018).

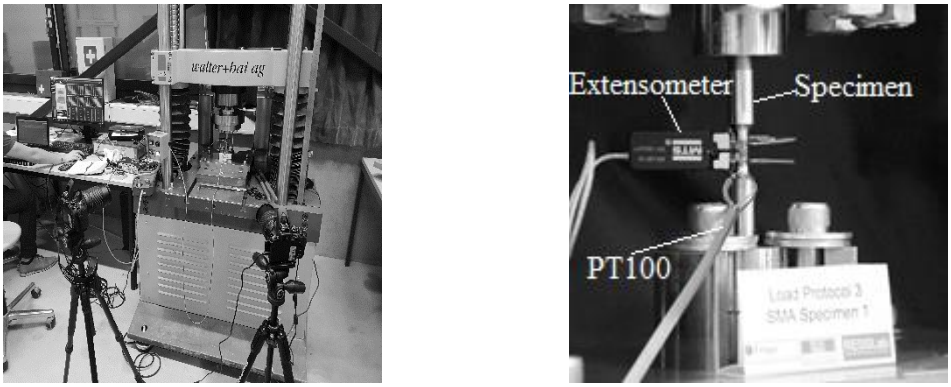

(a) Experimental setup (b) Detailed view of the specimen

Figure 1. Test apparatus and detailed view of round bar coupon specimens

The test is controlled using a Proportional-Integral-Derivative (PID) algorithm with a Walther & Bai PCS8000 controller. The first part of all tests up to $0.65f_y$ (where f_y denotes the nominal yield stress of the material) is conducted in load control. Tests are controlled by an MTS extensometer

up to a maximum of 12.5 % strain, which is the limit of the extensometer. For higher strains, tests are cross-head displacement-controlled.

2.2 Load Protocols

The load protocols (LPs) used to evaluate the Fe-SMA are selected from the work of Lignos & Suzuki (2013), in which they quantified response histories for a specific A992 Gr. 50 steel (nominal yield stress, f_y=355MPa). The LPs were developed on the basis of nonlinear response history analyses of steel moment resisting frame systems (Suzuki and Lignos 2014). In brief, the constant amplitude protocol is representative of long-duration ground motions that tend to cycle a structure symmetrically at fairly small inelastic drift cycles. The incremental protocols are deemed to be representative of ordinary and far-field records scaled at design basis seismic intensities (i.e., 10% probability of exceedance over 50 years) that cycle a structure symmetrically (i.e., mean effects tend to be zero or close to zero).

Loading rates are stipulated by international material testing standards (EN 10002-1: CEN 2001; and *ASTM* 2013); therefore, the strain rate of 0.03 %/sec and 0.8%/sec are selected as discussed in De Castro e Sousa & Lignos, (2018). An additional strain rate of 8%/sec is used which deemed to be analogous with that expected in steel structures subjected to earthquake loading (Lamarche & Tremblay, 2011). Five tests are shown as they are considered to be representative by showing key features of the material behavior under cyclic tension/compression loading.

- LP3: consists of one cycle at 4% strain amplitude and then tension until specimen fracture
- LP5_SR: consists of 50 cycles with a constant strain of 2% in tension and compression, with a strain rate of 0.03%/sec
- LP5_MR: consists of 50 cycles with a constant strain of 2% in tension and compression, with a strain rate of 0.8%/sec
- LP5_FR: consists of 10 cycles with a constant strain of 2% in tension and compression, with a strain rate of 8%/sec, then the specimen was left to cool down and then 50 more cycles were done with the same strain and strain rates
- LP7: consists of incrementally increasing strain amplitude of 1% until 8% strain with a strain rate of 0.03%/sec until 2% strain and 0.8 %/sec after.

3 RESULTS AND DISCUSSION

In this section, the results of the tests are presented and discussed. Figures 2 to 4 show the true stress – true strain and true strain-temperature from the tests. Figure 5 shows the first and last cycles of LP5 with different strain rates.

Referring to Figures 2(a) and 4(a) (LP3 and LP7, respectively), there is a small jump in the stress when the strain rate changes from 0.03%/sec to 0.8%/sec. This suggests that the material response is strain-rate dependent as there is an increase in the stress of 35 MPa while the strain rate increases. However, the influence of strain-rate on the resultant stress is similar with that seen in mild steels (Wakabayashi, et al. 1984 and Lamarche & Tremblay, 2011). Moreover, the stress peaks do not increase significantly when the strain rate increases. For instance, in Figure 5(a) the peaks of the first cycle differ by 30 MPa between the slow and the fast strain rates.

Referring to Figure 3 (b), (d) and (f), the measured temperature at the center of the gauge length increases with a higher rate while the strain rate increases. At high strain rates, the heat has less time to dissipate compared to low strain rates. For example, Figure 3(f) shows that for a strain rate of 8%/sec, the specimen's temperature increases up to 100 °C, while Figure 3(a) shows that the specimen's temperature reaches only 25 °C at a strain rate of 0.03%/sec.

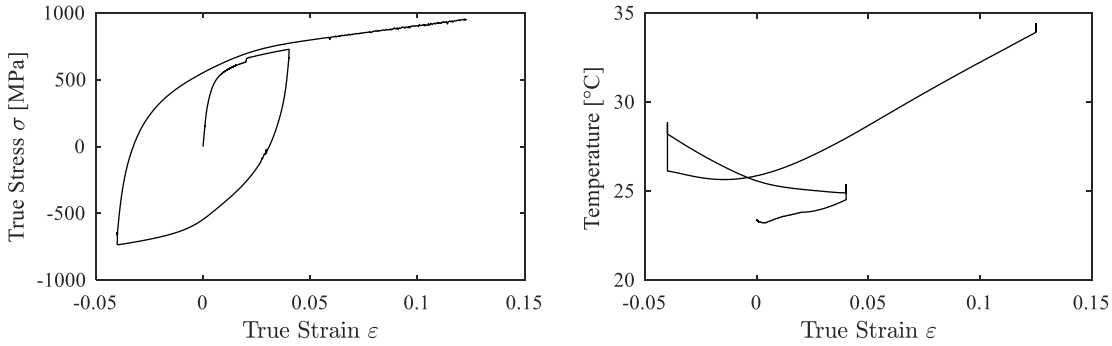

(a) True stress-true strain LP3 (b) True strain-temperature LP3

Figure 2. Material behavior under LP3 (0.03%/sec)

The slow-rate 2 % constant strain amplitude test (LP5_SR; Figure 3(a)) reveals that there is cyclic hardening of around 50 MPa, but only in tension. This is not significant as the increase is low compared to the value of the stress peak of 600 MPa (approximately 8 % increase over the course of 50 cycles). However, the hardening behavior of the material seems to be significantly strain-rate and/or temperature dependent, at least qualitatively. Referring to Figure 3(c), for LP5_MR (0.8%/sec), there is practically no isotropic hardening, while in Figure 3(e), for LP5_FR (8%/sec), there is cyclic softening of around 50 MPa in both in tension and compression after 30 cycles. The reason for this issue is still under investigation.

Figure 5(a) suggests that for small strain ranges (+/-2%) there are three distinct slopes in the corresponding true stress-true strain relationship when the material experiences compressive stresses. These slopes do not appear on the tensile side, thereby indicating an asymmetry in the material's hysteretic behavior. The change of the slope of the stress-strain relationship depends on the amount of irreversible work. The change in slope can be seen for the first three cycles prior to the 3 % strain amplitude. On the other hand, for higher strain amplitudes (after 3 %), the above issue becomes negligible. This is evident in Figure 4(a) that shows the material response under incrementally increasing strain amplitude up to 8% strain amplitude (LP7). The observed asymmetry in the material response is still under investigation.

The experimental data suggest that the Fe-SMA does not exhibit a super-elastic behavior even when the specimen's temperature increased to 100 °C under high-rate cyclic straining. This is shown in Figures 3(e) and 3(f). This observation is relevant in that it provides a bound on which one can reliably model the studied Fe-SMA without taking into account temperature-induced super-elasticity. At outset, this observation could not be reached so far as this temperature is in a range in which stress-induced reversible phase changes could occur, an observation reported in the experimental work conducted by Lee et al. (2013).

Referring to Figures 3(d) and 4(b), tests conducted with fairly similar strain rates indicate that the temperature rise is not dependent on the imposed loading protocol. In both examined cases, the temperature stabilized at about 40°C (i.e., temperature rise of about 20°C).

Despite the fact that the hysteretic shape of the examined Fe-SMA possesses some differences compared to that of mild steels, the potential for energy dissipation through inelastic cyclic straining between the two is fairly similar. However, its application into supplemental damping devices should be further examined.

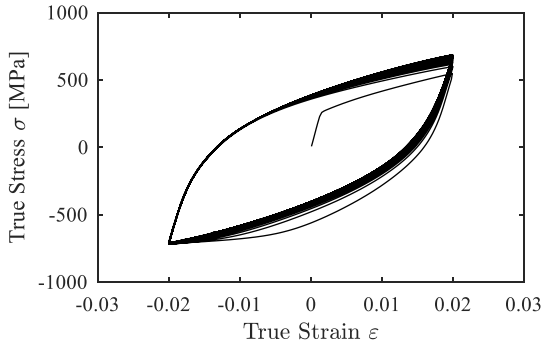

(a) True stress-true strain LP5_SR

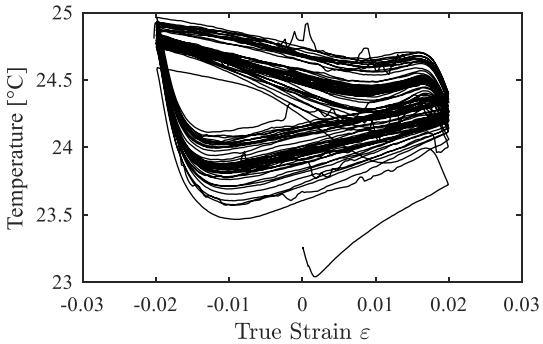

(b) True strain-temperature LP5_SR

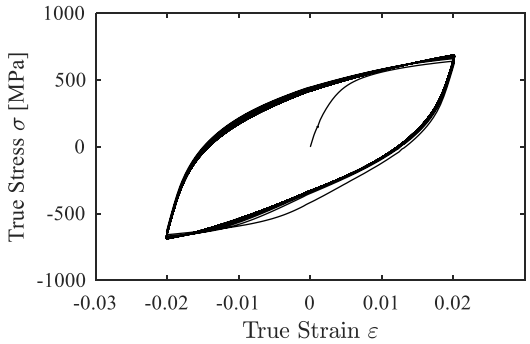

(c) True stress-true strain LP5_MR

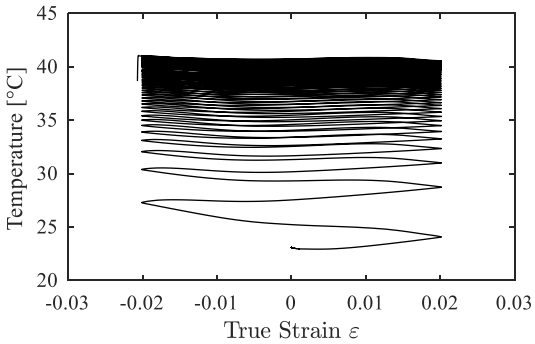

(d) True strain-temperature LP5_MR

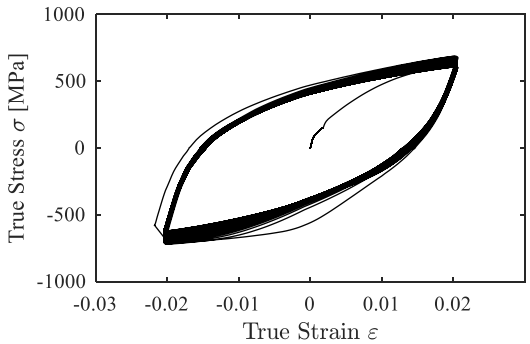

(e) True stress-true strain LP5_FR

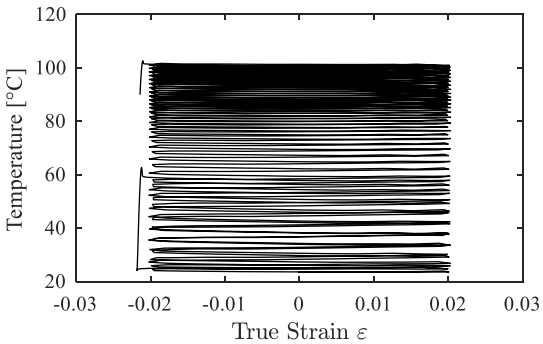

(f) True strain-temperature LP5_FR

Figure 3. Material behavior under LP5 – influence of strain rate on the true stress- true strain and true strain-temperature relationships

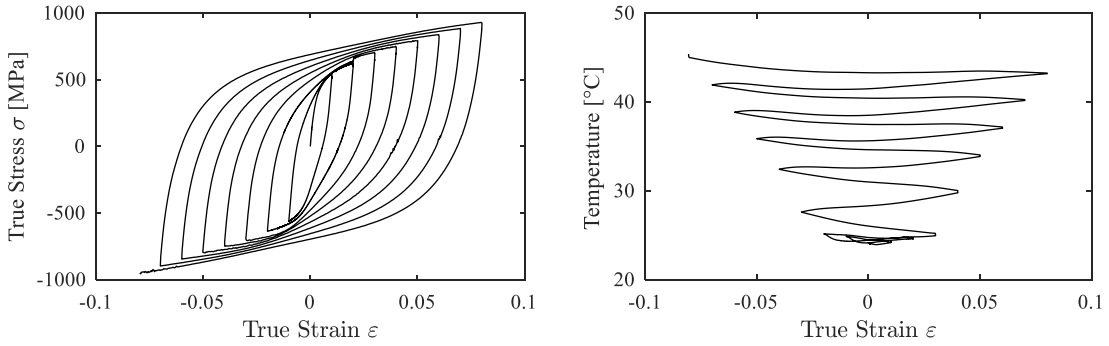

(a) True stress-true strain LP7 (b) True strain-temperature LP7

Figure 4. Material behavior under LP7 (0.03%/sec until 2% strain, 0.8% after)

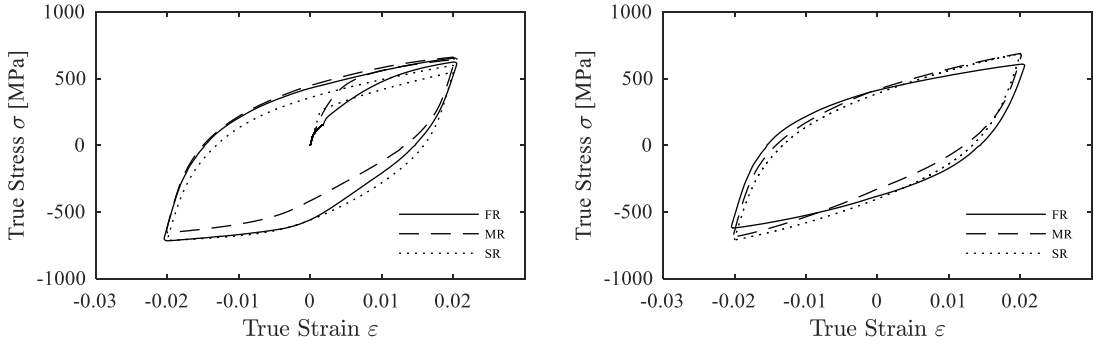

(a) First cycle (b) Last cycle (50th cycle)

Figure 5. Comparison of true stress-true strain relationship for LP5 at different strain-rates

4 SUMMARY AND OBSERVATIONS

In this paper, the behavior of an Fe-SMA under cyclic loading was characterized and discussed. Important features of this material were highlighted and explained. Understanding these features is essential in order to assess the suitability of this material for seismic applications. The main observations are summarized as follows:

- For a given loading protocol, a 100 °C temperature rise is observed at 8 %/sec, compared to 25 °C for at 0.03 %/sec. At high strain rates, the round bar coupon specimen has less time to dissipate heat compared to low strain rates.
- At low strain rates (0.03%/sec) for the 2% constant strain amplitude test, limited cyclic hardening of 50 MPa was observed in tension while no cyclic hardening was observed in compression. The cyclic hardening was found to be strain-rate dependent. For instance, at 0.8%/ sec, there was almost no hardening, while at 8 %/sec, there was softening of about 50 MPa both in tension and compression. This issue is still under investigation by the authors.
- The explored material does not indicate super-elastic behavior at room temperature with strains rates of up 8%/s, a value close to strain rates within a typical steel structure under earthquake loading.

- Tests conducted at relatively small strain amplitudes (+/-2%) suggest that the true stress-true strain material response in compression is characterized by three distinct slopes. This is not evident in tension. As such, the hysteretic material behavior is asymmetric. However, at larger strain amplitudes (strain amplitudes larger than 3%) this issue is not evident. This behavior aspect of the material is still under investigation by the authors.

The above observations are valuable for the proper representation of the Fe-SMA with a multi-axis constitutive law within the J_2 plasticity framework. While the asymmetry of the material response at smaller strain amplitudes should be considered, the thermomechanical aspect may be disregarded if its shape memory effect is not taken into consideration.

5 ACKNOWLEDGEMENTS

The authors graciously thank re-fer AG and Empa for the material and manufacturing of the Fe-SMA round bar coupon specimens used in this study. The second and third authors were supported by an EPFL internal grant. The financial support is gratefully acknowledged. Any opinions, findings, and conclusions or recommendations expressed in this paper are those of the authors and do not necessarily reflect the views of the sponsors.

6 REFERENCES

ASTM. *E8/E8M - 13a* (2013). *Standard Test Methods for Tension Testing of Metallic Materials 1*. West Conshohocken, PA, USA

Czaderski, C., Weber, B., Shahverdi, M., Motavalli, M., Leinenbach, C., Lee, W. Michels, J. (2015). Iron-based shape memory alloys (Fe-SMA) - a new material for prestressing concrete structures. *Proceedings of SMAR 2015 the 3rd conference on smart monitoring, assessment and rehabilitation of civil structures. Istanbul; Dubendorf: ITU; EMPA.*

De Castro e Sousa, A., & Lignos, D. (2018). Guidelines for uniaxial tests of steels under cyclic loading . Lausanne: EPFL.

Elkady, A., & Lignos, D. G. (2018). Full-scale testing of deep wide-flange steel columns under multiaxis cyclic soading: loading sequence, boundary effects, and lateral stability bracing force demands. *Journal of Structural Engineering*, *144*(2), 04017189.

CEN. (2001). *EN 10002-1:2001 - Metallic materials Tensile testing Part 1: method of test at ambient temperature*. Brussels, Belgium. European Committee for Standardization

Ghafoori, E., Hosseini, E., Leinenbach, C., Michels, J., & Motavalli, M. (2017). Fatigue behavior of a Fe-Mn-Si shape memory alloy used for prestressed strengthening. *Materials & Design*, *133*, 349-362.

Hosseini, E., Ghafoori, E., Leinenbach, C., Motavalli, M., & Holdsworth, S. R. (2018). Stress recovery and cyclic behaviour of an Fe–Mn–Si shape memory alloy after multiple thermal activation. *Smart Materials and Structures*, *27*(2), 025009.

Lamarche, C.-P., & Tremblay, R. (2011). Seismically induced cyclic buckling of steel columns including residual-stress and strain-rate effects. *Journal of Constructional Steel Research*, *67*(9), 1401-1410.

Lee, W. J., Weber, B., Feltrin, G., Czaderski, C., Motavalli, M., & Leinenbach, C. (2013). Phase transformation behavior under uniaxial deformation of an Fe–Mn–Si–Cr–Ni–VC shape memory alloy. *Materials Science and Engineering: A*, *581*, 1-7.

Lignos, D., & Suzuki, Y. (2013). Collapse assessment of steel frames designed with high-performance steel materials. Ph.D. Thesis Montreal, Canada: McGill University.

McCormick, J., DesRoches, R., Fugazza, D., & Auricchio, F. (2007). Seismic assessment of concentrically braced steel frames with shape memory alloy braces. *Journal of Structural Engineering*, *133*(6), 862-870.

Miller, D. J., Fahnestock, L. A., & Eatherton, M. R. (2012). Development and experimental validation of a nickel–titanium shape memory alloy self-centering buckling-restrained brace. *Engineering Structures*, *40*, 288-298.

Nikulin, I., Sawaguchi, T., Kushibe, A., Inoue, Y., Otsuka, H., & Tsuzaki, K. (2016). Effect of strain amplitude on the low-cycle fatigue behavior of a new Fe–15Mn–10Cr–8Ni–4Si seismic damping alloy. *International Journal of Fatigue*, *88*, 132-141.

Nikulin, I., Sawaguchi, T., Ogawa, K., & Tsuzaki, K. (2014). Low-cycle fatigue behavior and microstructural evolution of the Fe–30Mn–4Si–2Al Alloy. *Materials Science Forum*, *783-786*, 944-949.

Nikulin, I., Sawaguchi, T., & Tsuzaki, K. (2013). Effect of alloying composition on low-cycle fatigue properties and microstructure of Fe–30Mn–(6−x)Si–xAl TRIP/TWIP alloys. *Materials Science and Engineering: A*, *587*, 192-200.

Sawaguchi, T., Maruyama, T., Otsuka, H., Kushibe, A., Inoue, Y., & Tsuzaki, K. (2016). Design Concept and Applications of Fe-Mn-Si-based alloys; from shape-memory to seismic response control. *Materials Transactions*, *57*(3), 283-293.

Sawaguchi, T., Nikulin, I., Ogawa, K., Sekido, K., Takamori, S., Maruyama, T., Tsuzaki, K. (2015). Designing Fe–Mn–Si alloys with improved low-cycle fatigue lives. *Scripta Materialia*, *99*, 49-52.

Speicher, M. S., DesRoches, R., & Leon, R. T. (2011). Experimental results of a NiTi shape memory alloy (SMA)-based recentering beam-column connection. *Engineering Structures*, *33*(9), 2448-2457.

Wakabayashi, M., Nakamura, T., Iwai, S., & Hayashi, Y. (1984). Effects of strain rate on the behavior of structural members subjected to earthquake forces. *8th World Conference on Earthquake Engineering*. San Francisco, CA, USA.